

Cavity quantum electrodynamics of nanoscale two-level systems

B. Sarabi,^{1,2} A. N. Ramanayaka,^{1,2} A. L. Burin,³ F. C. Wellstood,^{2,4} and K. D. Osborn^{1,4}

¹Laboratory for Physical Sciences, College Park, MD 20740, USA

²Department of Physics, University of Maryland, College Park, MD 20742, USA

³Department of Chemistry, Tulane University, New Orleans, LA 70118, USA

⁴Joint Quantum Institute, University of Maryland, College Park, MD 20742, USA

(Dated: September 3, 2022)

Amorphous solids contain nanoscale two-level systems (TLSs) which are of interest in quantum computing because they are a source of decoherence but also can be used as a coherent resource. Here we report on a measurement of individual TLSs using cavity quantum electrodynamics (CQED). A superconducting resonator forms the cavity and an insulating-thickness film contains the TLSs. For a dielectric volume of $80 \mu\text{m}^3$, an individual TLS can be observed, and in silicon nitride we obtain a coherence time of $3.2 \mu\text{s}$, with vacuum Rabi states containing a 0.37 MHz splitting as a result of CQED strong coupling. The CQED system allows a photon-intensity study of the strongly coupled TLS, in the presence of weakly-coupled TLSs and with a comparison to theory.

Cavity quantum electrodynamics (CQED) phenomena, including vacuum Rabi splittings [1] and enhanced spontaneous emission [2], have greatly advanced the study of quantum levels in atoms [3], ions [4, 5] and superconducting qubits [6–8]. While the performance of the latter is limited by nanoscale tunneling two-level systems (TLSs) in amorphous solids [9–11], these low-energy excitations have also served as local quantum memories [12]. As a result, qubit characterization of TLSs, including their coherence times [13–15], is important but also has previously been limited to alumina, the prevalent Josephson junction tunneling barrier. While ensemble measurements of most amorphous solids reveal a similar density of TLSs, surprising deviations have been found in amorphous silicon and silicon nitride [16, 17], such that it is desirable to individually characterize TLSs in these materials for quantum coherent devices.

Here we report on a CQED study with TLSs, which allows us to characterize an individual TLS in an insulating-thickness film. In our experiment, the cavity is a circuit resonator made from a trilayer capacitor containing amorphous silicon nitride dielectric and a multi-turn superconducting inductor. Similar to some amorphous silicon, the type of silicon nitride deviates from the so-called universal loss observed in most other glasses. By using microscopic volumes of this material, we reach the CQED strong-coupling regime and observe vacuum Rabi splittings below a single (average) photon in the cavity. At higher photon numbers we observe saturation of the strongly-coupled TLS, and we also observe an interesting crossover between these two regimes, which results in a wishbone-shaped transmission. A theoretical simulation shows agreement with the nonlinear transition phenomena, and analysis allows us to extract the loss associated with weakly-coupled TLSs, which also begin saturation near a single photon in the cavity.

Microwave resonators, each containing an inductor and a capacitor, were made with trilayer capacitors having dielectric volumes (V) ranging from 80 to $5000 \mu\text{m}^3$ (see

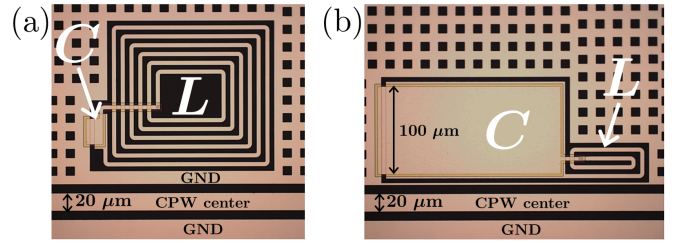


FIG. 1. Optical image of capacitor C and inductor L for resonators with (a) the smallest ($80 \mu\text{m}^3$) and (b) the largest ($5000 \mu\text{m}^3$) dielectric volumes. Aluminum appears light and sapphire substrate appears black.

Fig. 1). Despite having substantially different volumes, the resonance frequencies were kept in the 4.6 to 6.9 GHz range. The resonators were fabricated from superconducting aluminum films with a 250 nm thick film of amorphous hydrogenated silicon nitride ($\text{a-SiN}_x\text{:H}$) forming the capacitor dielectric [17]. Five resonators were fabricated on a chip and coupled (both inductively and capacitively) to a $20 \mu\text{m}$ wide transmission line resulting in a multi-band bandstop transmission.

Each resonator's transmission (S_{21}) was measured at 25 mK in a dilution refrigerator with on-resonance cavity photon numbers (\bar{n}) ranging from approximately 10^{-4} to 10^3 . For the two resonators with the largest insulator volumes, 5000 and $2500 \mu\text{m}^3$, a standard analysis technique of the resonances [18] yielded a low-power loss tangent of $\tan \delta_0 \simeq 1 \times 10^{-4}$ (see Fig. 5). At this low-temperature limit, the loss tangent depends on the electric field amplitude (E) in the dielectric approximately as $\tan \delta = \tan \delta_0 / \sqrt{1 + (E/E_c)^2}$. This follows from the standard model of TLSs [19, 20] with excitation energy $\mathcal{E} = \sqrt{\Delta^2 + \Delta_0^2}$ and standard TLS distribution $d^3N = (P_0/\Delta_0)d\Delta d\Delta_0 dV$ where N is the TLS number, P_0 is a material parameter, and Δ_0 represents the tunneling energy. Δ denotes the offset energy between the two wells, which is perturbed by the interaction energy

$\mathbf{p} \cdot \mathbf{E} = pE \cos \theta$ of the TLS dipole moment \mathbf{p} , which is at an angle θ with respect to the electric field \mathbf{E} . We measure $E_c = 4.6$ V/m for the two largest-volume resonators, and the same value is expected for both resonators since E_c is an intensive parameter inversely proportional to a characteristic TLS coherence time for large TLS ensemble (or sample volume) measurements [21].

For the smallest volume insulator, at $80 \mu\text{m}^3$, transmission (S_{21}) at low photon numbers in the resonator ($\bar{n} \ll 1$) showed a second resonant absorption amplitude (see Fig. 2). This second dip is consistent with a single TLS strongly interacting with the cavity. Two intermediate volume resonators, at 230 and $760 \mu\text{m}^3$, also showed features consistent with discrete TLSs, but their analysis will not be presented here due to space limitations. Because these devices exhibit CQED effects due to their volumes, we refer to them as micro- V resonators. The transmission is inconsistent with a dense background of weakly coupled TLSs, suggesting that we have achieved the strong CQED coupling limit, and also the limit where one dominant TLS is within the resonator bandwidth. We now examine how the micro- V resonator can exhibit a single strongly-coupled TLS.

The average number of TLSs (\bar{N}) in the bandwidth (B) of the micro- V resonator with $V = 80 \mu\text{m}^3$ can be estimated using the standard TLS distribution. The TLSs from the Δ - Δ_0 energy diagram which lie near a quarter circle equal to the microwave photon energy $\hbar\omega$ can interact strongly with the resonator. Using a representative angle of θ , we estimate the number of TLSs available for strong coupling as $\bar{N} \simeq 2\pi P_0 V \hbar B$. For a resonator cavity critically coupled to the internal loss tangent set by the TLSs, we get $B \propto \tan \delta_0$ hence $N \propto \tan^2 \delta_0$. Using $\tan \delta_0 = 10^{-4}$, we find that the number in the bandwidth is much lower than if we had alumina from either air-exposed ALD [22] or large-area Josephson junctions [9]. Using the resonator's external coupling and estimating $P_0 = 3\epsilon_0 \epsilon_r \tan \delta_0 / \pi p^2$ and the measured value of p from silicon nitride [23], we find $\bar{N} \simeq 1$ observable TLS in the smallest micro- V resonator, a value consistent with the data taken from multiple cooldowns.

To better understand our results, we examined a theoretical model of this micro- V device. The model has two cavities and one dominant TLS (Fig. 3). Cavity c represents the resonator which is strongly-coupled to the dominant TLS with rate g and weakly-coupled to many TLSs which produce the relaxation rate γ_c . Meanwhile, cavity c is coupled to a low- Q cavity d , which allows us to model our experimental setup [17] using a connection to two semi-infinite transmission lines, coupled by rates γ_1 and γ_2 [24]. This results in the modified Jaynes-Cummings Hamiltonian [25]

$$\begin{aligned} \mathcal{H} = & \hbar\omega_d d^\dagger d + \hbar\omega_c c^\dagger c + \hbar\Omega(d^\dagger c + c^\dagger d) \\ & + i\hbar g(S^+ c - c^\dagger S^-) + \mathcal{E}S^z. \end{aligned} \quad (1)$$

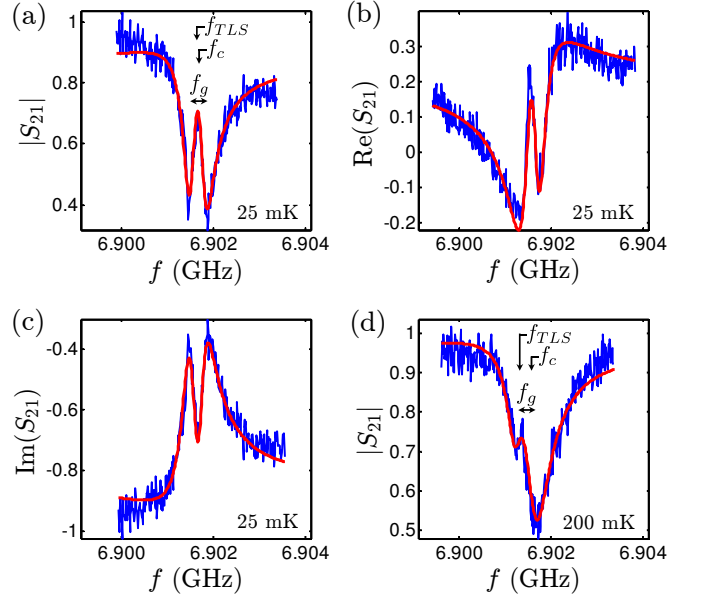


FIG. 2. (a) Measured $|S_{21}|$ vs. frequency f (blue) and optimum fit (red) at 25 mK. (b) and (c) show corresponding real and imaginary parts of S_{21} . (d) Measured (blue) and best fit (red) of $|S_{21}|$ vs. frequency at 200 mK. f_c and f_{TLS} are the cavity and TLS frequencies respectively, and $f_g = 2g/2\pi$ shows the vacuum Rabi frequency.

At small average photon numbers in cavity c , $\bar{n} \ll 1$, and in the low-temperature limit ($k_B T \ll \hbar\omega$), the dominant TLS, represented by the spin operator S^z , can be treated as an oscillator. At higher temperatures ($k_B T \gtrsim \hbar\omega$) we used a mean field approach and replace S^z with its thermodynamic average $\langle S^z \rangle = -\frac{1}{2} \tanh(\hbar\omega_0/2k_B T)$. The single-photon transmission, appropriate for $\bar{n} \ll 1$ is

$$S_{21} \simeq \frac{\sqrt{\gamma_1 \gamma_2}}{i(\omega - \omega_d) + \frac{\gamma_1 + \gamma_2}{2} + \frac{\Omega^2}{i(\omega - \omega_c) + \Gamma_c/2}}, \quad (2)$$

where

$$\Gamma_c = \gamma_c + \frac{2g^2 \tanh(\hbar\omega/2k_B T)}{i(\omega - \omega_{TLS}) + \gamma_{TLS}/2}. \quad (3)$$

Γ_c includes cavity damping (γ_c) from weakly-coupled TLSs and a complex term, related to the dominant TLS coupling

$$g = \frac{\Delta_0}{\mathcal{E}} p \cos \theta \sqrt{\frac{\omega_0}{2\epsilon_r \epsilon_0 \hbar V}}, \quad (4)$$

which allows a second resonance. These two resonances correspond to the transition energies from ground state ($n = 0$) to two excited states in the cavity- c /TLS system. Then from the second and last two terms in Eq. 1, the two lowest transition energies become $\Delta E_{n=0,\pm} = \hbar(\omega_c + \delta/2) \pm \hbar\sqrt{g^2 + (\delta/2)^2}$, where $\delta = \omega_{TLS} - \omega_c$. From Eq. 3 it follows that a single TLS at resonance with the

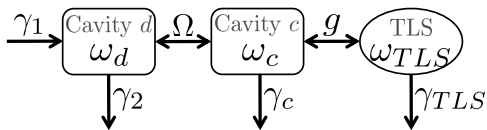


FIG. 3. Model of micro-V device. Cavity c (the resonator) is coupled to cavity d with rate Ω , and to the dominant TLS with rate g . Each cavity and the TLS has a characteristic resonance frequency ω_d , ω_c and ω_{TLS} , and cavity c and the TLS have relaxation rates γ_c and γ_{TLS} , respectively.

cavity can be distinguished if its maximum response exceeds the average response of the weakly-coupled TLSs, *i.e.* $\chi = \pi P_0 \hbar V / 6 T_1 < 1$, where $T_1 = 1/\gamma_{TLS}$ is the TLS relaxation time. Comparing Eq. 2 with the familiar Lorentzian transmission [18] yields the internal, external and total quality factors of the resonator as $Q_c = \omega_c/\gamma_c$, $Q_e = \omega_c(\gamma_1 + \gamma_2)/4\Omega^2$ and $Q = 1/(Q_c^{-1} + Q_e^{-1})$, respectively.

Fig. 2(a)-(c) show a fit to the data using the low-temperature limit of Eq. 2 and the Least-Squares Monte Carlo (LSM) method. To reduce the number of fitting parameters, we assume $Q_d = \omega_d/\gamma_d = 20$ and set $\gamma_1 = \gamma_2 = \gamma_d/2$ for cavity d . Analysis of Eq. 2 near ω_c shows that these assumptions do not affect the fit parameters of cavity c and the TLS for $Q_d \ll Q_c$. The LSM fit made to $\text{Re}(S_{21})$ and $\text{Im}(S_{21})$ is shown in Fig. 2(b) and 2(c), while Fig. 2(a) shows $|S_{21}|$. The fit yields $\omega_d/2\pi = 6.978419$ GHz and $\gamma_d = 2.19$ GHz for cavity d , $f_c = \omega_c/2\pi = 6.901689$ GHz and $\gamma_c = 1.92$ MHz for cavity c , $f_{TLS} = \omega_{TLS}/2\pi = 6.901629$ GHz and $T_2 = 2/\gamma_{TLS} = 3.2 \mu\text{s}$ for the TLS, where the latter is the coherence time of the resonant TLS including the decay at rate γ_{TLS} from spontaneous emission and neglecting dephasing. This silicon nitride TLS coherence time is at least 3 times larger than previously characterized individual TLSs [14, 15], and will be discussed further below.

The intercavity coupling rate is $\Omega = 41.9$ MHz, $Q_e \simeq 14000$, and the coupling of cavity c to the TLS under consideration is $g = 1.15$ MHz. Also, from Eq. 4 we obtain a transition dipole moment of $p_{min} = (\Delta_0/\mathcal{E})p \cos \theta = 1.6$ Debye. This minimum extracted dipole size for the strongly-coupled TLS is consistent with previous work [23]. The spontaneous photon emission time, calculated from p_{min} and Q_e , is comparable to the extracted relaxation time, indicating that T_2 may be limited by the photon rather than phonon emission.

In Fig. 2(d) we show the data to the same micro-V device at $T = 200$ mK. We also show the fit to the data with cavity d parameters and intercavity coupling Ω set equal to the low temperature results. The fit reveals $g = 1.13$ MHz, and that it is almost unaffected by temperature, while $f_{TLS} = 6.901318$ GHz and $f_c = 6.901576$ GHz have a small shift due to weak influence from TLS, as expected. Unlike at low temperature,

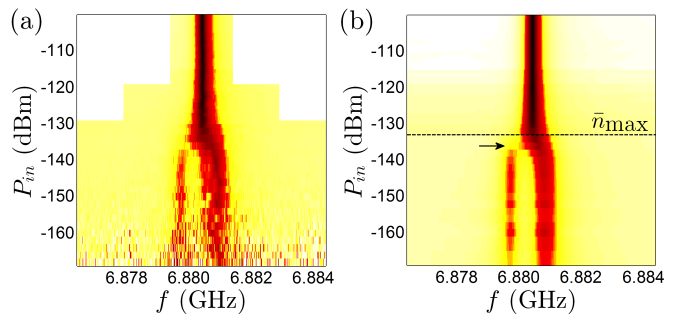


FIG. 4. (a) False-color plot showing measured transmission $|S_{21}|$ vs. input power P_{in} and frequency f for the micro-V resonator with $V = 80 \mu\text{m}^3$. (b) Simulated power dependence from theoretical fit to model. $\bar{n}_{\text{max}} \simeq 7$ indicates the photon number above which the simplified dual-cavity model is used and the arrow shows the break of $n > 1$ transitions.

δ is now comparable to g (see the markings in Fig. 2(d)). This causes uneven superposition of the bare states, and causes the transition to the high-energy cavity-like state $E_{n=0,+}$ to have a larger amplitude than $E_{n=0,-}$. Still, the other TLS-like state is visible to the left of the cavity-like state. Using Eq. 3 with the remaining fit values, $T_1(200 \text{ mK}) = 0.57 \mu\text{s}$ and γ_c , allows us to calculate the ratio of the TLS-like state signal on the background of the cavity-like state as $4g^2 \tanh(\hbar\omega_{TLS}/2k_B T) T_1/\gamma_c = 0.67$, where $\tanh(\hbar\omega/2k_B T) = 0.68$. The $T_1(200 \text{ mK})$ reveals a faster TLS decay than expected from the increased phonon emission which scales as $\tanh(\hbar\omega/2k_B T)$ and predicts $T_1(200 \text{ mK}) = 1.1 \mu\text{s}$. However, this is qualitatively consistent with spectral diffusion, which causes TLS dephasing [26], or the parabolic temperature dependence of TLS coherence times found in alumina tunneling barriers [15].

Fig. 4(a) shows a false-color plot of $|S_{21}|$ (measured at 25 mK) as a function of frequency and input power P_{in} , from a different cooldown in the micro-V device. For $P_{in} < -135$ dBm we observe the two vacuum Rabi states from the transition energies involving the ground state, similar to those shown Fig. 2, expected from a low-power probe of the $n = 0 \rightarrow 1$ (single photon) excitation of the system. At higher powers we generally expect other transitions due to the Poisson distribution from \bar{n} in cavity c . Eq. 1 gives four transition energies $\Delta E_{n>0,\pm,\pm} = \hbar\omega_c \pm \hbar\sqrt{g^2(n+1) + (\delta/2)^2} \mp \hbar\sqrt{g^2 n + (\delta/2)^2}$ from the n th hybridized pair $|n, g\rangle, |n-1, e\rangle$ to that of the next higher energy. The high-power central dip corresponds to the $\Delta E_{n>0,+,+}$ and $\Delta E_{n>0,-,-}$ transitions, which asymptotically approach a single frequency ($\hbar\omega_c$) for large n , while $\Delta E_{n>0,+,-}$ and $\Delta E_{n>0,-,+}$ do not.

Now with the low power ($\bar{n} \ll 1$) and high-power ($\bar{n} \gg 1$) regimes understood, we next explain the crossover ($\bar{n} \sim 1$), including a break on the left part of the wishbone (see the arrow marking in Fig. 4 (b)). At low powers, notice that similar to Fig. 2(d), there is a larger ampli-

tude for the high frequency transition, and once again this is caused by a cavity-like transition for $\Delta E_{n=0,+}$. In addition, the high-power transition $\Delta E_{n>0,+}$ is closer to $\Delta E_{n=0,+}$, than $\Delta E_{n>0,-}$ is to $\Delta E_{n=0,-}$, for a given $n > 0$. Then, the apparent break (continuity) of the low (high) frequency crossover from low to high power is expected due to the more (less) spectrally diffuse transition energies than the other high (low) frequency one.

A detailed analysis was performed using a density matrix simulation with an arbitrary number of photons at zero temperature. The simulation uses the Lindblad equations with the Hamiltonian of Eq. 1. We find parameters for cavities c and d by fitting the high-power data ($\bar{n} > \bar{n}_{\max} \simeq 7$) where the strongly coupled TLS is power-saturated and a classical-field analysis is allowed. This can be equivalently described by Eq. 2 with $g = 0$. As before, we assume $Q_d = 20$ and $\gamma_1 = \gamma_2 = \gamma_d/2$. The parameters of the fit are $\gamma_d = 2.17$ GHz and $\Omega = 41.6$ MHz, showing excellent consistency with the previously found values. The extracted γ_c decreases with power due to saturation of the weakly-coupled TLSs. Also, we obtain $\omega_c/2\pi = 6.880434$ GHz and $\omega_d/2\pi = 6.899807$ GHz. The small shift in ω_c with respect to the previous cooldown could be explained by a 0.6% change in the aluminum inductance relative the cooldown from Fig. 2, and the sole difference is that the micro- V device is sensitive to a TLS with slightly lower energy. Next, we fit the data for $\bar{n} < \bar{n}_{\max}$, where \bar{n}_{\max} is close to our computational limit, using the above values for cavity d and c to extract the dominant TLS parameters and low-power γ_c values. From this, we obtain $\omega_{TLS}/2\pi = 6.880106$ GHz, $\gamma_{TLS} = 3.08$ MHz and $g = 3.14$ MHz. The theoretical plot with the extracted parameters is shown in Fig. 4(b) for the entire measurement power range, which was -170 to -100 dBm entering the device, corresponding to maximum photon storage values (on resonance) of $10^{-4} \lesssim \bar{n} \lesssim 10^3$.

Furthermore, the cavity loss tangent $\tan \delta = \gamma_c/\omega_c$ can be obtained for the entire power span using the extracted γ_c values. Fig. 5 compares $\tan \delta$ for the micro- V ($80 \mu\text{m}^3$) resonator with the large-volume ($5000 \mu\text{m}^3$) resonator from the same chip. While both resonators show $\tan \delta_0 \simeq 1 \times 10^{-4}$, analysis of the data shows $E_c = 13.6$ V/m for the micro- V device which is 3 times larger than that of the large-volume resonator mentioned above. Interestingly, for the micro- V device, the critical number of photons calculated from E_c is $\bar{n}_c = 0.2$, such that the beginning of saturation for the TLS environment is reached in a quantum regime. While quantum effects on the weakly-coupled TLSs must be present, we expect inherent TLS-sampling variations to cause \bar{n}_c to vary such that it may be desirable to try many TLS configurations using electric field bias control in the future [23]. We note that quantum effects of loss saturation have been theoretically analyzed previously only for a single TLS [27]. For a full analysis, one expects complex dynamics

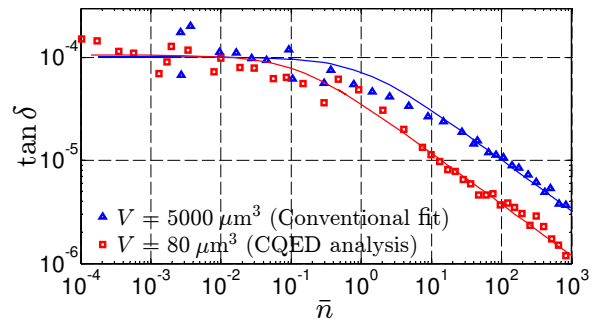


FIG. 5. Loss tangent extracted from CQED power-dependent analysis.

similar to other coupled-spin problems [28, 29], due to the distribution of TLS pseudospins in this experiment.

In conclusion, we have measured and characterized individual nanoscale TLSs after achieving the CQED strong coupling regime. This was accomplished with lumped-element superconducting resonators with microscopic electric field volumes made of amorphous silicon nitride. In the low-temperature limit, a vacuum Rabi splitting of 0.37 MHz is observed and the strongly interacting TLS was found to have a coherence time of $T_2 = 3.2 \mu\text{s}$, which is longer than that of the TLSs previously observed within tunneling barriers. In a photon-intensity study, the two low-energy transitions, which reveal the vacuum Rabi splitting, are observed to crossover to the high-power cavity transitions, with an explicable break between these regimes on the low-frequency side. The relaxation and coupling parameters of the hybrid system were extracted for the entire measurement power span using a theoretical model.

The incredibly long TLS coherence time is possibly caused by the properties of our thick insulating silicon nitride film. This T_2 time is similar to that of the original transmon qubit plus cavity [30]. To add frequency tuning to the TLS, one could incorporate electric field tuning [23] in the capacitance, and this would create a very small TLS qubit plus resonator system due to the nanoscale TLS and the resonator with a multiturn inductor.

There are two possible causes for the larger coherence time relative to TLSs in superconducting qubits: alumina may have a stronger bulk phonon coupling, or the thin tunneling barriers which they are studied in may cause an enhanced phonon (strain-field) coupling compared to the bulk value of alumina due to a surface effect. This study shows that by using microscopic volumes of materials, individual TLSs in insulating-thickness films can be characterized using CQED.

The authors thank M. S. Khalil, C. J. Lobb, M. J. A. Stoutimore, B. Palmer, Y. Rosen and S. Gladchenko for many useful discussions. A. Burin acknowledges support through Army Research Office Grant vv911NF-13-1-0186, the LA Sigma Program, and the NSF EPCORE

LINK Program.

-
- [1] J. J. Sanchez-Mondragon, N. B. Narozhny, and J. H. Eberly, *Phys. Rev. Lett.* **51**, 1925 (1983).
- [2] P. Goy, J. M. Raimond, M. Gross, and S. Haroche, *Phys. Rev. Lett.* **50**, 1903 (1983).
- [3] Y. Kaluzny, P. Goy, M. Gross, J. M. Raimond, and S. Haroche, *Phys. Rev. Lett.* **51**, 1175 (1983).
- [4] J. I. Cirac and P. Zoller, *Phys. Rev. Lett.* **74**, 4091 (1995).
- [5] D. Leibfried, R. Blatt, C. Monroe, and D. Wineland, *Rev. Mod. Phys.* **75**, 281 (2003).
- [6] A. Wallraff, D. I. Schuster, A. Blais, L. Frunzio, R.-S. Huang, J. Majer, S. Kumar, S. M. Girvin, and R. J. Schoelkopf, *Nature* **431**, 162 (2004).
- [7] A. Blais, R.-S. Huang, A. Wallraff, S. M. Girvin, and R. J. Schoelkopf, *Phys. Rev. A* **69**, 062320 (2004).
- [8] M. D. Reed, L. DiCarlo, B. R. Johnson, L. Sun, D. I. Schuster, L. Frunzio, and R. J. Schoelkopf, *Phys. Rev. Lett.* **105**, 173601 (2010).
- [9] J. M. Martinis, K. B. Cooper, R. McDermott, M. Steffen, M. Ansmann, K. D. Osborn, K. Cicak, S. Oh, D. P. Pappas, R. W. Simmonds, and C. C. Yu, *Phys. Rev. Lett.* **95**, 210503 (2005).
- [10] R. W. Simmonds, K. M. Lang, D. A. Hite, S. Nam, D. P. Pappas, and J. M. Martinis, *Phys. Rev. Lett.* **93**, 077003 (2004).
- [11] K. B. Cooper, M. Steffen, R. McDermott, R. W. Simmonds, S. Oh, D. A. Hite, D. P. Pappas, and J. M. Martinis, *Phys. Rev. Lett.* **93**, 180401 (2004).
- [12] M. Neeley, M. Ansmann, R. C. Bialczak, M. Hofheinz, N. Katz, E. Lucero, A. Oconnell, H. Wang, A. Cleland, and J. M. Martinis, *Nat. Phys.* **4**, 523 (2008).
- [13] Z. Kim, V. Zaretsky, Y. Yoon, J. F. Schneiderman, M. D. Shaw, P. M. Echternach, F. C. Wellstood, and B. S. Palmer, *Phys. Rev. B* **78**, 144506 (2008).
- [14] Y. Shalibo, Y. Rofe, D. Shwa, F. Zeides, M. Neeley, J. M. Martinis, and N. Katz, *Phys. Rev. Lett.* **105**, 177001 (2010).
- [15] J. Lisenfeld, C. Müller, J. H. Cole, P. Bushev, A. Lukashenko, A. Shnirman, and A. V. Ustinov, *Phys. Rev. Lett.* **105**, 230504 (2010).
- [16] D. R. Queen, X. Liu, J. Karel, T. H. Metcalf, and F. Hellman, *Phys. Rev. Lett.* **110**, 135901 (2013).
- [17] H. Paik and K. D. Osborn, *Appl. Phys. Lett.* **96**, 072505 (2010).
- [18] M. S. Khalil, M. J. A. Stoutimore, F. C. Wellstood, and K. D. Osborn, *J. Appl. Phys.* **111**, 054510 (2012).
- [19] P. W. Anderson, B. I. Halperin, and C. M. Varma, *Philos. Mag.* **25**, 1 (1972).
- [20] W. Phillips, *J. Low. Temp. Phys.* **7**, 351 (1972).
- [21] M. V. Schickfus and S. Hunklinger, *Phys. Lett. A* **64**, 144 (1977).
- [22] M. S. Khalil, M. J. A. Stoutimore, S. Gladchenko, A. M. Holder, C. B. Musgrave, A. C. Kozen, G. Rubloff, Y. Q. Liu, R. G. Gordon, J. H. Yum, S. K. Banerjee, C. J. Lobb, and K. D. Osborn, *Appl. Phys. Lett.* **103**, 162601 (2013).
- [23] M. S. Khalil, S. Gladchenko, M. J. A. Stoutimore, F. C. Wellstood, A. L. Burin, and K. D. Osborn, *arXiv:1312.4865* (2013).
- [24] M. J. Collett and C. W. Gardiner, *Phys. Rev. A* **30**, 1386 (1984).
- [25] E. Jaynes and F. W. Cummings, *P. IEEE* **51**, 89 (1963).
- [26] J. L. Black and B. I. Halperin, *Phys. Rev. B* **16**, 2879 (1977).
- [27] M. Bhattacharya, K. D. Osborn, and A. Mizel, *Phys. Rev. B* **84**, 104517 (2011).
- [28] L. Faoro and L. B. Ioffe, *Phys. Rev. Lett.* **109**, 157005 (2012).
- [29] J. Shao and P. Hänggi, *Phys. Rev. Lett.* **81**, 5710 (1998).
- [30] A. Houck, J. Koch, M. Devoret, S. Girvin, and R. Schoelkopf, *Quantum Inf. Process.* **8**, 105 (2009).